Design and Implementation of a Tree-Based Blind Modulation Classification Algorithm for Multiple-Antenna Systems

Rahul Gupta, Sudhan Majhi, *Senior Member, IEEE*, and Octavia A. Dobre, *Senior Member, IEEE*

***Abstract*— This paper presents the design and testbed implementation of a tree-based algorithm, which classifies many of the linearly modulated signals, such as binary phase-shift keying (PSK), quadrature PSK (QPSK), offset QPSK, $\pi/4$-QPSK, 8-PSK, minimum shift keying, and 16-quadrature amplitude modulation. The proposed modulation classification algorithm is applicable to spatially multiplexed multiple antenna systems over frequency-selective fading channels. It works in the presence of timing, phase, and frequency offsets, without having prior knowledge of the channel state information. Classification is performed by utilizing the combined properties of the correlation functions, cyclic cumulant (CC), and cumulant. The correlation function of the received baseband signal exhibits peaks at a particular set of time lag, which represents distinctive features for the modulation formats. The CC uses the position of nonzero cycle frequency of the received baseband signals to classify modulation formats, while the cumulant employs threshold values. To authenticate the proposed algorithm, implementation and measurement are performed in an indoor propagation environment by using a National Instrument testbed setup. The performance of the proposed algorithm is compared with existing methods via Monte Carlo simulations.**

***Index Terms*— Correlation function, cumulant, cyclic cumulant (CC), modulation classification (MC), testbed implementation.**

I. Introduction

BLIND modulation classification (MC) is a class of signal processing techniques with numerous applications, such as spectrum surveillance, signal intelligence, electronic surveillance, emitter interception, electronic warfare, as well as control and network management. Several theoretical studies have been carried out over the past decades [1], but only a few have been implemented and validated in realistic scenarios [2]–[7]. Algorithms for blind parameter estimation and signal classification can be used with a smart receiver, yielding an increase in the spectral efficiency by reducing the overhead.

In recent years, interest in MC algorithms has increased significantly, where the success rate of the classification algorithm has to be high for reliable communication. The MC algorithms can be divided into two general categories: likelihood based and feature based. The MC for single-input single-output (SISO) systems has been comprehensively explored in [1] and references therein. Likelihood-based algorithms [8] require knowledge of signal parameters, i.e., carrier frequency, symbol rate, and timing offset. Thus, parameter estimation needs to be performed prior to MC. The estimation and measurement of a carrier frequency in multipath propagation environment are discussed in [9]–[11]. The experimental studies of estimating the symbol rate for bandlimited signals are given in [6], where a modified second-order cyclic cumulant (CC) has been used over a fading channel. The prediction and measurement of time synchronization and signal bandwidth over practical scenarios also play an important role while classifying the modulation formats [12]–[15]. In general, the implementation and measurement of MC algorithms without prior knowledge of signal parameters and channel state information (CSI) are highly desirable for future intelligent communication systems [3]. The feature-based statistical methods, such as those employing moments, cumulants, and CCs, have been widely used in the literature to accomplish such requirements [2], [16]–[25]. The higher order CCs are robust and many of them perform well even in frequency-selective fading channels; however, the CC and cumulant-based algorithms implemented in [2] and [19] are for flat fading channel and additive white Gaussian noise (AWGN). In addition, all these methods are restricted to SISO systems only.

Nowadays, the multiple-input multiple-output (MIMO) technology is used in the wireless systems. Spatial multiplexing and space–time coding added advantages include increase in the data rate by transmitting several information streams in parallel and diversity gain, respectively. Practical challenges, implementation, and measurement of spatial multiplexed multiple antenna systems have been studied in [26] and [27]. Recently, MC algorithms for multiple antenna systems have gained more attention for cognitive radios and a few works have been presented in the literature [28]–[35]. MC algorithms based on expectation–maximization, machine learning, higher order moment, and CCs are studied in [29]–[33]. The higher order moments and cumulants-based methods in [31] and [32] are limited to the case when the number of transmit antennas

Manuscript received May 3, 2018; revised August 23, 2018; accepted August 24, 2018. This work was supported in part by the Visvesvaraya Young Faculty Research Fellowship, Ministry of Electronics and Information Technology, Government of India, being implemented by the Digital India Corporation and Early Career Young Scientists by the Science and Engineering Research Board under the Department of Science and Technology, Government of India, and in part by the Natural Sciences and Engineering Research Council of Canada through its Discovery Program. The Associate Editor coordinating the review process was Huang-Chen Lee. *(Corresponding author: Octavia A. Dobre.)*

R. Gupta and S. Majhi are with the Department of Electrical Engineering, IIT Patna, Patna 801103, India (e-mail: rahul.pee15@iitp.ac.in; smajhi@iitp.ac.in).

O. A. Dobre is with the Department of Electrical and Computer Engineering, Memorial University, St. John's, NL A1B 3X9, Canada (e-mail: odobre@mun.ca).

Color versions of one or more of the figures in this paper are available online at http://ieeexplore.ieee.org.

Digital Object Identifier 10.1109/TIM.2018.2868556

is lower or equal to the number of receive antennas. The method based on the higher order correlation function discussed in [34] and [35] is applicable to any number of transmit and receive antennas over frequency-selective fading channels, without having prior knowledge of the CSI. However, the features employed by these methods are the same for quadrature phase-shift keying (QPSK) and its variants, i.e., offset QPSK (OQPSK), $\pi/4$-QPSK, and minimum shift keying (MSK). Thus, it is not possible to distinguish these modulations by using the existing methods. To the best of our knowledge, there exists no MC algorithm in the literature which can be applied to different variants of QPSKs and 8-PSK together, for multiple antenna systems over frequency-selective fading channel.

In this paper, we propose a novel tree-based MC using the statistical properties of different modulation schemes. The proposed algorithm has important features, as follows.

1) It can be applied to a more comprehensive pool of modulations, i.e., binary PSK (BPSK), QPSK, $\pi/4$-QPSK, OQPSK, 8-PSK, MSK, and 16-quadrature amplitude modulation (QAM). Moreover, classifying 8-PSK and $\pi/4$-QPSK together is another major problem which has been addressed in this paper.
2) In the proposed algorithm, new features are obtained to classify 8-PSK, QPSK, and its variants. The features are extracted by employing the correlation functions, CC, and cumulant.
3) It is applicable to SISO, single-input multiple-output (SIMO), multiple-input single-output (MISO), and MIMO systems over frequency-selective channels in the presence of timing, phase, and frequency offsets, without the requirement of CSI.
4) Its performance is measured in an indoor propagation environment to validate the proposed algorithm.
5) The complexity of the proposed algorithm is less than for the maximum likelihood (ML) algorithm but greater than that of the algorithms based on cumulant and correlation function. Moreover, the algorithms based on the ML, cumulant, and correlation function cannot classify 8-PSK and different variants of the QPSK modulation formats.

The rest of this paper is organized as follows. Section II introduces the model of the received discrete-time baseband signal. Section III describes the proposed MC algorithm based on the properties of higher order correlation function, second-order CC, and fourth-order cumulant. In this section, the theoretical derivations of CC and the proposed tree-based MC algorithm are introduced. Section IV presents the measurement setup in an indoor propagation environment. Simulation and measurement results are provided in Section V. Finally, this paper is concluded in Section VI.

II. Signal Model

We consider a spatially multiplexed MIMO system with N_t transmit and N_r receive antennas. In this paper, we assume the case of colocated multiple antennas, and only a single common frequency and phase offset appear in the different transmit–receive antenna pairs [36]. The received discrete-time baseband signal at the mth receive antenna is expressed as

$$y_m[n] = e^{j(2\pi f_0 n+\phi)} \sum_{q=0}^{N_t-1} \sum_{l=0}^{L-1} h_{qm}[l] x_q[n-l-\tilde{N}_1] + w_m[n] \tag{1}$$

where f_0 is the frequency offset normalized to the symbol rate, ϕ is the phase offset, $h_{qm}[l]$ is the fading channel coefficient between the qth transmit and mth receive antennas, $l = 0, \ldots, L-1$, with L as the maximum number of channel taps, $\tilde{N}_1$ is the number of samples corresponding to the timing offset, and $w_m[n]$ is the AWGN at the mth receive antenna. The transmitted signal from the qth transmit antenna can be written as

$$x_q[n] = x_{q_r}[n] + j x_{q_i}[n] \tag{2}$$

where the I and Q components of $x_q[n]$ are given as $x_{q_r}[n] = \sum_{k=0}^{K-1} a_{q_r}[k] g[n-kP]$, $x_{q_i}[n] = \sum_{k=0}^{K-1} a_{q_i}[k] g[n-kP-\tilde{N}_2]$, with K as the number of symbols and $a_q[k] = a_{q_r}[k] + j a_{q_i}[k]$ as the kth symbol drawn from any of the considered modulation schemes at the qth transmitted antenna. For BPSK : $a_{q_r}[k] = \pm 1, a_{q_i}[k] = 0$, and for $\{\text{QPSK}, \text{OQPSK}, \text{MSK}\}$: $a_{q_r}[k], a_{q_i}[k] = \pm 0.7071$, with $\tilde{N}_2 = P/2$ for OQPSK and MSK and zero otherwise. Furthermore, MSK is a special case of OQPSK with sinusoidal pulse weighting as given in Section III-B1, $\{\pi/4-\text{QPSK}, 8-\text{PSK}\} : a_{q_r}[k], a_{q_i}[k] = \pm 1, \pm 0.7071$, and $16-\text{QAM} : a_{q_r}[k], a_{q_i}[k] = \pm 3/\sqrt{10}, \pm 1/\sqrt{10}$. The transmitted pulse shape $g[n]$ is root raised cosine (RRC) and the oversampling factor is defined as $P = F_s/f_s = T/T_s = N/K$, where F_s is the sampling rate, $f_s = 1/T$ is the symbol rate, T is the symbol period, $T_s = 1/F_s$ is the sampling period, and N is the received signal length.

III. Proposed Blind Modulation Classification Algorithm

The statistical tools, i.e., higher order moment, cumulant, and correlation functions have strong properties to classify BPSK, M-ary PSK (M-PSK), and M-QAM [31]–[35]. However, they are unable to classify the other variants of PSK, i.e., OQPSK, $\pi/4$-QPSK, MSK, and 8-PSK modulation formats together. On the other hand, second-order CC provides distinct features for classifying these PSK variants. To classify all seven modulation formats, a tree-based algorithm is proposed and implemented by utilizing the combined properties of the correlation functions, CC, and cumulant function at each level of the tree in Sections III-A–III-D.

A. First-Level Classification

It has been shown that the correlation functions of the received baseband signals exhibit peaks at a particular set of time lag and can be used to extract distinct features for modulation formats. To classify BPSK versus the other modulation formats, we use the following second-order correlation function [34]:

$$A_{m,m'}(p) = \mathrm{E}[y_m(n) y_{m'}(n+p)] \tag{3}$$

where p is the time lag between two signals and $m, m' \in 0, 1, \ldots, N_r-1, m \neq m'$. After substituting (1) into (3) and using the general assumptions that the data symbols are uncorrelated

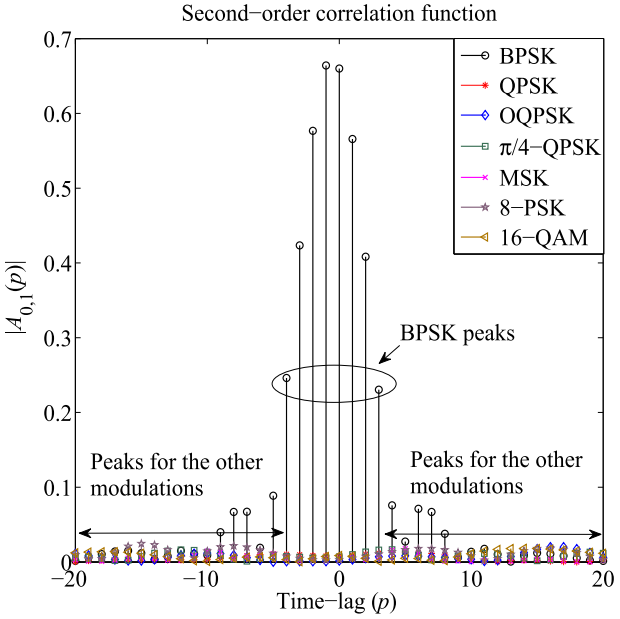

Fig. 1. Magnitude of the second-order correlation function of the received signal for $L = 4$, $K = 1000$, and $P = 10$ for the seven modulation formats.

with zero mean, and the noise in each channel is independent of the others [17], one can write that [34]

$$A_{m,m'}(p) = \begin{cases} e^{j(2\pi f_0(2n+p)+2\phi)} \sum_{q=0}^{N_t-1} \sum_{l,l'=0}^{L-1} h_{qm}[l]\, h_{qm'}[l'] \\ \times x_q[n-l]x_q[n-l']\delta[p+l-l'], \quad \text{for BPSK} \\ 0, \quad \text{otherwise} \end{cases} \tag{4}$$

where $\delta(.)$ is the Kronecker delta function. From (4), it is observed that the BPSK modulation format exhibits peaks for $A_{m,m'}(p)$ at $p \in \{-(L-1), \ldots, (L-1)\}$, and there are no significant peaks for the rest of the modulation formats; only those due to the estimation errors resulting from the use of a finite number of symbols, as illustrated in Fig. 1 for $K = 1000$ and $P = 10$.

B. Second-Level Classification

To classify the rest of the modulation formats (except BPSK), we use the statistical property of the second-order CC [23], [37], [38] along with the experimental and measurement framework of the second-order cyclostationarity [24]. The mathematical derivation of the second-order CC for different modulation formats is described in the following.

1) Second-Order CC for MSK Modulated Signal: The I and Q components of the transmitted MSK signal at the qth transmit antenna can be expressed as

$$x_{q_r}[n] = \sum_{k=0}^{K-1} a_{q_r}[k]g[n-kP]\cos(\pi n/P) \tag{5a}$$

$$x_{q_i}[n] = \sum_{k=0}^{K-1} a_{q_i}[k]g[n-kP-P/2]\sin(\pi n/P). \tag{5b}$$

Now, the second-order time-varying correlation function of the received complex baseband signal with zero time lag is defined as

$$c_{y_m}[n;0] = \mathrm{E}\big[y_m[n]y_m^*[n]\big] \tag{6}$$

which for the I component can be expressed as

$$\begin{aligned} c_{y_{m_r}}[n;0] &= \sum_{q=0}^{N_t-1}\sum_{l=0}^{L-1} \big|h_{qm}[l]\big|^2 \sum_{k=0}^{K-1}\sum_{k'=0}^{K-1} \mathrm{E}\big[a_{q_r}(k)a_{q_r}^*(k')\big] \\ &\quad \times g[n-l-kP-\tilde{N}_1]g[n-l-k'P-\tilde{N}_1] \\ &\quad \times \cos^2[\pi n/P] + \sigma^2_{w_{m_r}} \\ &= \frac{\sigma^2_{a_{q_r}}}{4P} \sum_{q=0}^{N_t-1}\sum_{l=0}^{L-1} \big|h_{qm}[l]\big|^2 \sum_{k=0}^{K-1} G[k/P]e^{j2\pi nk/P} \\ &\quad \times e^{-j2\pi k(\tilde{N}_1+l)/P}(e^{j2\pi n/P} + e^{-j2\pi n/P} + 2) \\ &\quad + \sigma^2_{w_{m_r}} \end{aligned} \tag{7}$$

where $\sigma^2_{a_{q_r}} = \mathrm{E}[|a_{q_r}[k]|^2]$, $\sigma^2_{w_{m_r}} = \mathrm{E}[|w_{m_r}[n]|^2]$, and $G[.]$ is the discrete Fourier transform (DFT) of $g^2[.]$. Note that the final expression of (7) is obtained by using the Poisson sum formula. The Fourier series coefficient of (7), $C_{y_{m_r}}[\alpha;0] = \lim_{N\to\infty} 1/N \sum_{n=0}^{N-1} c_{y_{m_r}}[n;0]e^{-j2\pi\alpha n}$, represents the CC at zero time lag and cycle frequency α if it satisfies $C_{y_{m_r}}[\alpha;0] \neq 0$. The consistent estimator of $C_{y_{m_r}}[\alpha;0]$ is obtained as

$$\begin{aligned} \tilde{C}_{y_{m_r}}[\alpha;0] &\triangleq \frac{1}{N}\sum_{n=0}^{N-1} c_{y_{m_r}}[n;0]e^{-j2\pi\alpha n} \\ &= \frac{\sigma^2_{a_{q_r}}}{4P} \sum_{q=0}^{N_t-1}\sum_{l=0}^{L-1}\sum_{k=0}^{K-1} G[k/P]|h_{qm}[l]|^2 \frac{1}{N}\sum_{n=0}^{N-1} \\ &\quad \times (e^{-j2\pi n(\alpha-k/P-1/P)} + e^{-j2\pi n(\alpha-k/P+1/P)} \\ &\qquad + 2e^{-j2\pi n(\alpha-k/P)})e^{-j2\pi k(\tilde{N}_1+l)/P} \\ &\quad + \frac{1}{N}\sum_{n=0}^{N-1} e^{-j2\pi n\alpha}\ \sigma^2_{w_{m_r}} \\ &= \frac{\sigma^2_{a_{q_r}}}{4P} \sum_{q=0}^{N_t-1}\sum_{l=0}^{L-1} |h_{qm}[l]|^2 \sum_{k=0}^{K-1} G[k/P] \\ &\quad \times e^{-j2\pi k(\tilde{N}_1+l)/P}(2\delta[\alpha-k/P] \\ &\quad + \delta[\alpha-k/P-1/P] + \delta[\alpha-k/P+1/P]) \\ &\quad + \sigma^2_{w_{m_r}}\delta[\alpha]. \end{aligned} \tag{8}$$

Because, the length of the received signal is limited, $\tilde{C}_{y_{m_r}}[\alpha;0]$ is seldom exactly zero even if α is not a cycle frequency, as shown in Fig. 2.

Now, for the Q component of the received complex baseband signal, $y_{m_i}[n]$, the second-order time-varying correlation function with zero time lag can be obtained as

$$\begin{aligned} c_{y_{m_i}}[n;0] &= \frac{\sigma^2_{a_{q_i}}}{4P} \sum_{q=0}^{N_t-1}\sum_{l=0}^{L-1} \big|h_{qm}[l]\big|^2 \sum_{k=0}^{K-1} G\,[k/P]\, e^{j2\pi nk/P} \\ &\quad \times e^{-j\pi k}\ e^{-j2\pi k(\tilde{N}_1+l)/P} \\ &\quad \times (2 - e^{j2\pi n/P} - e^{-j2\pi n/P}) + \sigma^2_{w_{m_i}} \end{aligned} \tag{9}$$

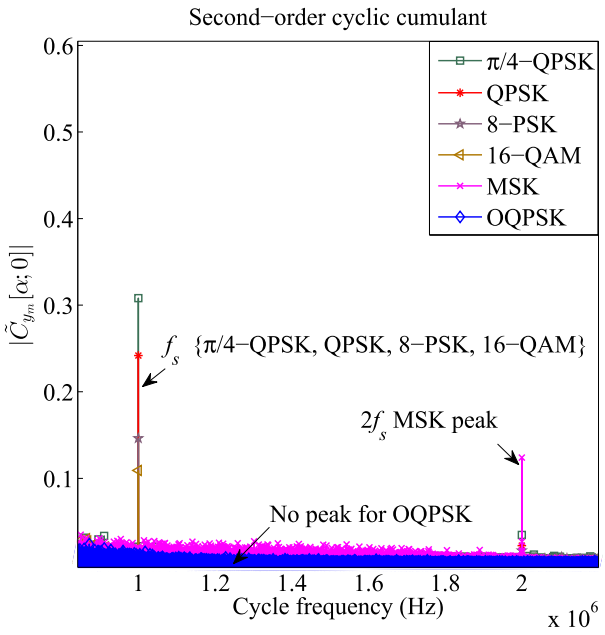

Fig. 2. Estimate of the second-order CC for QPSK, $\pi/4$-QPSK, MSK, OQPSK, 8-PSK, and 16-QAM modulated signals at $f_s = 1$ MHz.

where $\sigma^2_{a_{q_i}} = \mathrm{E}\big[|a_{q_i}[k]|^2\big]$ and $\sigma^2_{w_{m_i}} = \mathrm{E}[|w_{m_i}[n]|^2]$. Similarly, the estimator of the CC $C_{y_{m_i}}[\alpha;0]$ at zero time lag and cycle frequency α, can be expressed as

$$\tilde{C}_{y_{m_i}}[\alpha;0] = \frac{\sigma^2_{a_{q_i}}}{4P}\sum_{q=0}^{N_t-1}\sum_{l=0}^{L-1}|h_{qm}[l]|^2\sum_{k=0}^{K-1}G[k/P] \times e^{-j2\pi k(\tilde{N}_1+l)/P}\; e^{-j\pi k}\;(2\delta[\alpha-k/P] - \delta[\alpha-k/P-1/P]-\delta[\alpha-k/P+1/P]) + \sigma^2_{w_{m_i}}\delta[\alpha]. \quad (10)$$

Since a bandlimited filter is used, the CC $C_{y_m}[\alpha;0] = 0$ for $k > 1$ [6]. Thus, the estimator of the CC $C_{y_m}[\alpha;0]$ is obtained for $k = 0, 1$ as

$$\tilde{C}_{y_m}[\alpha;0] = \frac{1}{4P}\sum_{q=0}^{N_t-1}\sum_{l=0}^{L-1}|h_{qm}[l]|^2 \times\big\{2\delta[\alpha]\big(\sigma^2_{a_{qr}}+\sigma^2_{a_{q_i}}\big)+(\delta[\alpha-1/P] +\delta[\alpha+1/P])\big(\sigma^2_{a_{qr}}-\sigma^2_{a_{q_i}}\big)+G[1/P] \times e^{-j2\pi(\tilde{N}_1+l)/P}\big(2\delta[\alpha-1/P]\big(\sigma^2_{a_{qr}}-\sigma^2_{a_{q_i}}\big) +(\delta[\alpha-2/P]+\delta[\alpha])\big(\sigma^2_{a_{qr}}+\sigma^2_{a_{q_i}}\big)\big)\big\} +\sigma^2_{w_m}\delta[\alpha] \quad (11)$$

where $\sigma^2_{w_m} = \sigma^2_{w_{m_r}} + \sigma^2_{w_{m_i}}$. As the power of the I and Q components of $a_q[m]$ is the same, $\sigma^2_{a_{qr}} - \sigma^2_{a_{q_i}} = 0$, and the final expression is

$$\tilde{C}_{y_m}[\alpha;0] = \frac{1}{4P}\sum_{q=0}^{N_t-1}\sum_{l=0}^{L-1}|h_{qm}[l]|^2\big(\sigma^2_{a_{qr}}+\sigma^2_{a_{q_i}}\big) \times\{2\delta[\alpha]+G[1/P]\times e^{-j2\pi(\tilde{N}_1+l)/P} \times(\delta[\alpha-2/P]+\delta[\alpha])\}+\sigma^2_{w_m}\delta[\alpha]. \quad (12)$$

2) Second-Order CC for QPSK, $\pi/4$-QPSK, OQPSK, 8-PSK, and 16-QAM Modulated Signals: First, for classifying QPSK, $\pi/4$-QPSK, 8-PSK, and 16-QAM modulated signals, similarly, we derive the estimator of $C_{y_{m_r}}[\alpha;0]$ at zero time lag and cycle frequency α as

$$\tilde{C}_{y_{m_r}}[\alpha;0] = \frac{\sigma^2_{a_{qr}}}{P}\sum_{q=0}^{N_t-1}\sum_{l=0}^{L-1}|h_{qm}[l]|^2\sum_{k=0}^{K-1}G[k/P] \times e^{-j2\pi k(\tilde{N}_1+l)/P}\;\delta[\alpha-k/P]+\sigma^2_{w_{mr}}\delta[\alpha]. \quad (13)$$

A similar equation can be obtained for the Q component as well, and thus, for $k = 0, 1$, the estimator of the CC $C_{y_m}[\alpha;0]$ is obtained as

$$\tilde{C}_{y_m}[\alpha;0] = \frac{1}{P}\sum_{q=0}^{N_t-1}\sum_{l=0}^{L-1}|h_{qm}[l]|^2\big(\sigma^2_{a_{qr}}+\sigma^2_{a_{q_i}}\big) \times\{\delta[\alpha]+G[1/P]e^{-j2\pi(\tilde{N}_1+l)/P}\delta[\alpha-1/P]\} +\delta[\alpha]\sigma^2_{w_m}. \quad (14)$$

For the OQPSK modulated signals, $\tilde{N}_2 = P/2$, and the estimator of the CC for the Q component of the received baseband signal is obtained as

$$\tilde{C}_{y_{m_i}}[\alpha;0] = \frac{\sigma^2_{a_{q_i}}}{P}\sum_{q=0}^{N_t-1}\sum_{l=0}^{L-1}|h_{qm}[l]|^2\sum_{k=0}^{K-1}G[k/P]e^{-j\pi k} \times e^{-j2\pi k(\tilde{N}_1+l)/P}\;\delta[\alpha-k/P]+\sigma^2_{w_{m_i}}\delta[\alpha]. \quad (15)$$

Finally, the CC estimator expression of $y_m[n]$ for OQPSK modulated signal for $k = 0, 1$ is obtained as

$$\tilde{C}_{y_m}[\alpha;0] = \frac{1}{P}\sum_{q=0}^{N_t-1}\sum_{l=0}^{L-1}|h_{qm}[l]|^2 \times\big\{\delta[\alpha]\big(\sigma^2_{a_{qr}}+\sigma^2_{a_{q_i}}\big)+G[1/P] \times e^{-j2\pi(\tilde{N}_1+l)/P}\delta[\alpha-1/P]\big(\sigma^2_{a_{qr}}-\sigma^2_{a_{q_i}}\big)\big\} +\delta[\alpha]\sigma^2_{w_m}. \quad (16)$$

In (16), as the power of the I and Q components of $a_q[m]$ is the same, $\sigma^2_{a_{qr}} - \sigma^2_{a_{q_i}} = 0$, and the final expression is

$$\tilde{C}_{y_m}[\alpha;0] = \frac{1}{P}\sum_{q=0}^{N_t-1}\sum_{l=0}^{L-1}|h_{qm}[l]|^2\delta[\alpha]\big(\sigma^2_{a_{qr}}+\sigma^2_{a_{q_i}}\big)+\delta[\alpha]\sigma^2_{w_m}. \quad (17)$$

In practice, the CC estimate at zero time lag and cycle frequency α is simply calculated as [23]

$$\tilde{C}_{y_m}[\alpha;0] \triangleq \frac{1}{N}\sum_{n=0}^{N-1}|y_m[n]|^2e^{-j2\pi n\alpha}. \quad (18)$$

Equation (18) is the normalized DFT of $|y_m[n]|^2$ and can be implemented by the fast Fourier transform algorithm. Once $\tilde{C}_{y_m}[\alpha;0]$ is obtained, the frequency estimation is straightforward [23]

$$\hat{f}_m = \arg\max_{\alpha\in[u,v]}|\tilde{C}_{y_m}[\alpha;0]| \quad (19)$$

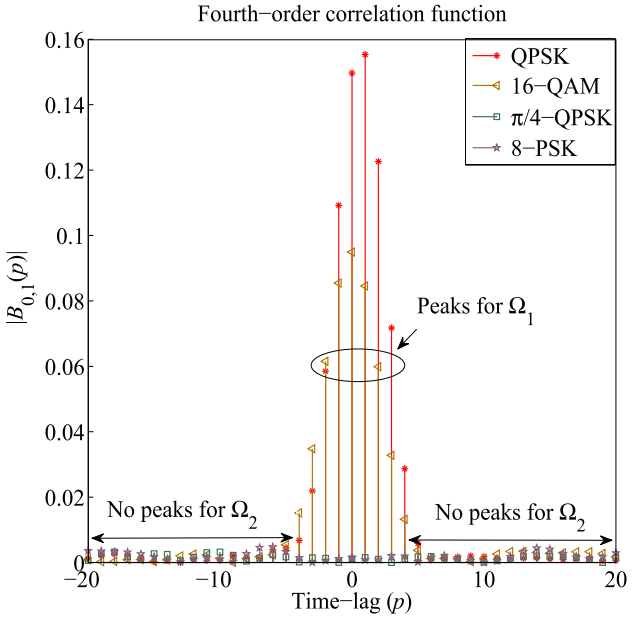

Fig. 3. Magnitude of the fourth-order correlation function for $L = 4$, $K = 10\,000$, and $P = 10$ for $\Omega_1 = \{\text{QPSK}, 16-\text{QAM}\}$ and $\Omega_2 = \{\pi/4-\text{QPSK}, 8-\text{PSK}\}$ modulated signals.

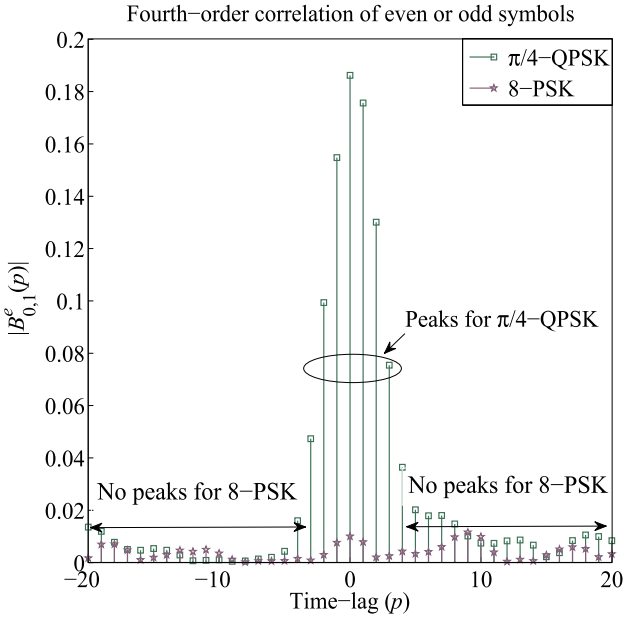

Fig. 4. Magnitude of the fourth-order correlation function of even or odd symbols for $L = 4$, $K = 20\,000$, and $P = 10$ for $\pi/4$-QPSK and 8-PSK modulated signals.

where $[u, v]$ is the lower and upper bound search interval, $u = \alpha_u N/F_s$ and $v = \alpha_v N/F_s$, $[\alpha_u, \alpha_v] \equiv [f_{bw}/2, f_{bw}/1.2]$; this interval is obtained through extensive simulation and measurement studies, with f_{bw} as the 3-dB signal bandwidth, obtained simply from the power spectral density of the received signal [4], [15]. As we deal with multiple antenna systems having N_r received antennas, we have $\hat{f}_m$ for $m = 0, \ldots, N_r - 1$ estimated frequencies. If any of the links is effected by deep fade, the other links provide the features for the classification of the modulation formats.

From (12), it is observed that a second-order CC peak for MSK modulated signal appears at $\alpha = 2/P$, i.e., at $2f_s$ as shown in Fig. 2. From (14), a second-order CC peak for QPSK, $\pi/4$-QPSK, 8-PSK, and 16-QAM modulated signals appears at $\alpha = 1/P$, i.e., at f_s. From (17), for OQPSK there is no peak, as shown in Fig. 2. Since QPSK, $\pi/4$-QPSK, 8-PSK, and 16-QAM do not have distinct features for the second-order CC, it is not possible to distinguish these modulation formats in the second-level classification stage. We further investigate their distinct features for the third-level classification stage.

C. Third-Level Classification

At this level, the fourth-order correlation function is used as a distinct feature for the classification of the modulation formats. This is defined as [34]

$$B_{m,m'}(p) = \mathrm{E}[(y_m[n])^2 (y_{m'}[n+p])^2] \tag{20}$$

where $m \neq m'$, $m, m' = 0, 1, \ldots, N_r - 1$. Now, substituting (1) into (20), $B_{m,m'}(p)$ can easily be expressed as given in [34]. From (20), it is found that QPSK and 16-QAM exhibits peaks, while $\pi/4$-QPSK and 8-PSK do not, as shown in Fig. 3 for $K = 10\,000$ and $P = 10$.

D. Fourth-Level Classification

At the final level, we have two sets of modulation formats $\Omega_1 = \{\text{QPSK}, 16-\text{QAM}\}$ and $\Omega_2 = \{\pi/4-\text{QPSK}, 8-\text{PSK}\}$, which need to be classified. For Ω_1, we use the fourth-order cumulant with two conjugations, $E_{y_m} = \text{cum}\left(y_m[n], y_m[n], y_m^*[n], y_m^*[n]\right)$ [19]. For N_r receive antennas, we take the average of all fourth-order cumulant as $E_{\text{avg}} = (1/N_r)\sum_{m=0}^{N_r-1} E_{y_m}$, such that the effect of the deep fade link is minimized. For QPSK, $E_{\text{avg}} \leq \Gamma_1$, while $E_{\text{avg}} > \Gamma_1$ for 16-QAM, where Γ_1 is a threshold decided through extensive simulation and measurement studies [19].

For Ω_2, first, we split the received baseband signal into odd $y_m^o[\hat{n}]$ and even $y_m^e[\tilde{n}]$ symbols as

$$y_m^o[n] = y_m[Pr + i_1], \quad r = 0, 2, 4, \ldots, N \tag{21a}$$
$$y_m^e[n] = y_m[Ps + i_1], \quad s = 1, 3, 5, \ldots, N-1 \tag{21b}$$

where $0 \leq i_1 < P$. Now, the fourth-order correlations of these symbols are given as

$$B_{m,m'}^o(p) = \mathrm{E}\left[\left(y_m^o[n]\right)^2 \left(y_{m'}^o[n+p]\right)^2\right] \tag{22a}$$
$$B_{m,m'}^e(p) = \mathrm{E}\left[\left(y_m^e[n]\right)^2 \left(y_{m'}^e[n+p]\right)^2\right] \tag{22b}$$

where $m \neq m'$, $m, m' = 0, 1, \ldots, N_r - 1$. For the $\pi/4$-QPSK modulation, separated even and odd symbols exhibit QPSK constellations rotated by $\pi/4$ with respect to each other. As such, (22a) and (22b) provide peaks for $\pi/4$-QPSK, while there are no peaks for 8-PSK, as shown in Fig. 4. The proposed tree-based MC algorithm is depicted in Fig. 5.

IV. Testbed Implementation and Measurement Setup

The testbed implementation and measurement transmission chain are separated into hardware and software parts.

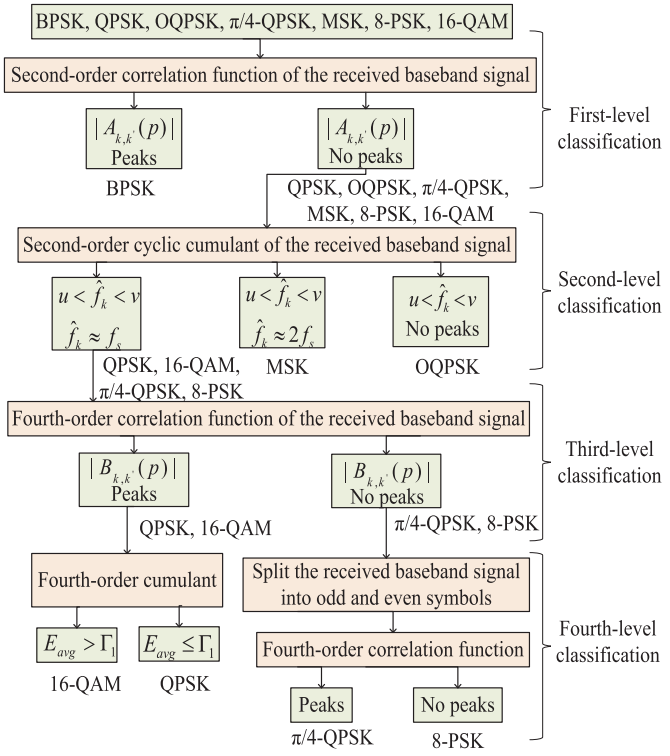

Fig. 5. Proposed tree-based MC algorithm.

(a) (b)

Fig. 6. NI PXIe-1075 chassis with NI PXIe-8135 embedded controller and the onboard modules at (a) transmitter with NI PXIe-5673 and (b) receiver with NI PXIe-5663 2×2 MIMO setup.

The hardware consists of two National Instruments (NI) Peripheral Component Interconnect (PCI) eXtensions for Instrumentation (PXIe)-1075 chassis: one at the transmitter and another one at the receiver. The transmitter is configured by using two NI PXIe-5673 vector signal generators (VSGs), and the receiver is configured by employing two NI PXIe-5663 vector signal analyzers (VSAs) [39]. The system has two VERT-2450 antennas at the transmitter and two antennas at the receiver, as shown in Fig. 6. The software consists of LabVIEW and MATLAB programing at the transmitter and receiver.

A. Laboratory Environment Setup

The implementation and measurements have been performed in the signal processing for wireless communication (SPWICOM) laboratory, which is located on the third floor

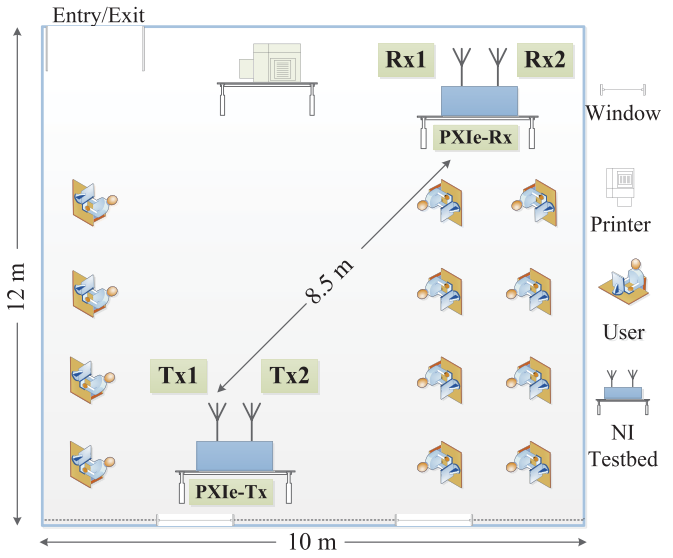

Fig. 7. Floor plan of the laboratory for the implementation and measurement setup.

of the Science block, at IIT Patna, Patna, India. The floor plan of the lab is shown in Fig. 7. SPWICOM is a typical modern office with width 10 m, length 12 m, and height 2.8 m. The laboratory has a number of workstations for students and staff. The environment in the laboratory is quite dynamic due to consistent human traffic. The transmitter and receiver antennas were installed at a height of 1.5 m from the floor level. The multipath propagation environment is considered between transmitter and receiver.

B. Testbed Hardware Setup

The NI PXIe-1075 chassis are equipped with NI PXIe-8135 embedded controller with a 2.3-GHz Intel i7 processor with 16-GB random access memory and are shown in Fig. 6. The system has two VERT-2450 dual band vertical antennas at the transmitter and two at the receiver. In addition, each antenna has a peak gain of 3 dBi, 50 Ohm impedance, with an omnidirectional radiation pattern.

1) Two Transmitter Hardware Setup: At the transmitter section, we have two NI PXIe-5673, i.e., VSG 1 and VSG 2; each consists of one NI PXIe-5450 dual-channel 16-bit arbitrary waveform generator and one NI PXIe-5611 radio frequency (RF) upconverter to transmit the signal through the air at 2.3 GHz. The NI PXIe-5611 RF upconverter is connected with the common NI PXI-5652 local oscillator (LO), an RF continuous wave source with a 500 kHz–6.6 GHz frequency range, as shown in Fig. 8. Two RF signals (Tx 1 and Tx 2) are generated by using the same modulations, pulse shaping filter parameters, and symbol rate. Pulse shaping is used to reduce the intersymbol interference; an RRC finite impulse response filter with a rolloff factor (β) of 0.5 and filter length 8 is employed. The signal bandwidth, $B_s = f_s(1+\beta)$, with f_s during the experiment equal to 5 MHz, results in a flat bandwidth of 7.5 MHz. For indoor propagation, typically, the delay spread in between 50 and 200 ns [40]. Hence,

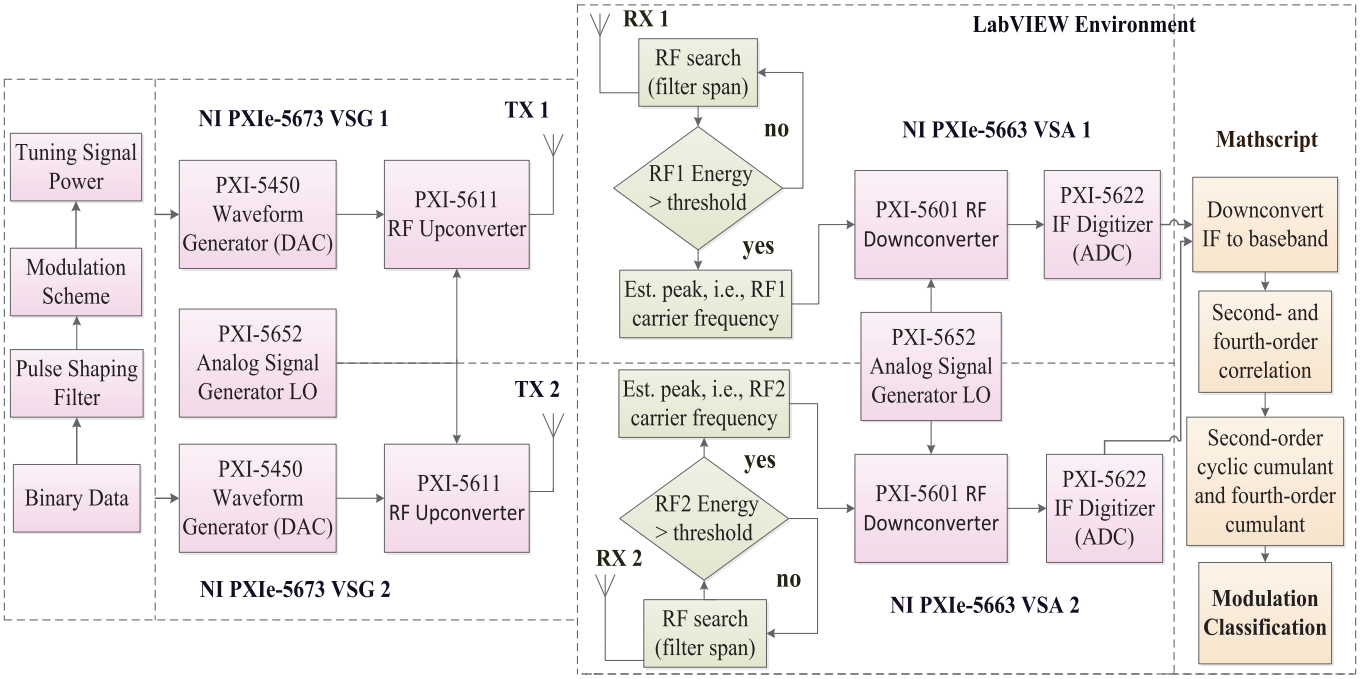

Fig. 8. Block diagram of transmitter signal acquisition, IF, and baseband signal processing in LabVIEW environment for 2 × 2 MIMO setup.

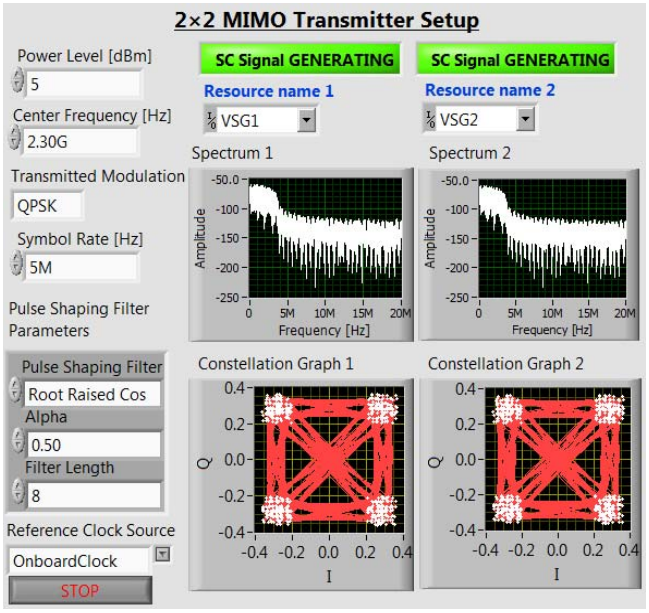

Fig. 9. LabVIEW front panel of the transmitter setup using PXIe-5673 for the 2 × 2 MIMO system.

the coherence bandwidth is 1–4 MHz. Thus, the transmitted signal experiences frequency-selective fading in the indoor propagation environment. The transmit power and RF carrier frequency can easily be changed through the front panel of the transmitter for a 2 × 2 MIMO system, as shown in Fig. 9.

The proposed MC algorithm is also tested with the Keysight VSG. The Keysight PXIe-M9019A chassis is equipped with M9037A four-slot PXIe embedded controller and M9381A PXIe-VSG. The Keysight M9381A PXIe-VSG consists of four PXIe modules, i.e., M9311A digital vector modulator, M9310A source output, M9301A synthesizer, and M9300A frequency reference [41]. The software used to configure these modules is the N7608B signal studio for custom modulation. Here, first, we configure the hardware by setting the carrier frequency and power (dBm). Next, in the waveform setup, we choose the custom modulation as custom in-phase and quadrature (IQ) or orthogonal frequency-division multiplexing or 5G candidate. The custom IQ signals are generated for different modulation formats, pulse shaping filter parameters, and symbol rates, and then, the signal is transmitted from the M9310A source output through the VERT-2450 antenna.

2) Two Receiver Hardware Setup: The receiver section is implemented by using the two NI PXIe-5663, i.e., VSA 1 and VSA 2, each consisting of one NI PXIe-5601 RF downconverter module, which downconverts an RF signal to an intermediate frequency (IF) and one NI PXIe-5622 16-bit IF digitizer. Both NI PXIe-5601 RF downconverters are connected to the common LO source, NI PXI-5652 RF continuous wave source, as shown in Fig. 8.

C. Modulation Classification Measurement

Both signal analyzers (VSA 1 and VSA 2) are separated into three sections: RF signal acquisition, IF, and baseband signal processing. The RF signal acquisition is processed through the LabVIEW signal analyzer modules. The IF and baseband signal processing are controlled by LabVIEW MathScript real-time (RT) module, as shown in Fig. 8.

1) RF Signal Acquisition: In the RF acquisition process, the two received RF signals (Rx 1 and Rx 2) are passed through a specified filter span, i.e., selected by the lower and upper values of the transmitted carrier frequency, to receive the

TABLE I
SIMULATION AND EXPERIMENT PARAMETERS OF THE SYSTEM

Simulation parameters	Value
Filter type	RRC
Roll-off factor β	0.5
Symbol rate f_s	5 MHz
Number of symbol K	20000
Carrier frequency f_c	5 MHz
Number of iteration	10000
Experimental parameters	
IF carrier frequency	5 MHz
RF carrier frequency	2.3 GHz
Receiver sampling rate F_s	50 MHz

signals within this band. For both signals, the received RF energy is measured and then compared with a predefined threshold. The threshold value is acquired through a receiver calibration process, by keeping the transmitter idle. If the energy of the received signal is above the predefined threshold, the position of the peak is estimated, which is the estimated RF carrier frequency; otherwise, the next signal burst is captured. Now, both received RF signals are downconverted to IF signal by their respective NI PXIe-5601 RF downconverter module by setting the LO frequency as (RF–IF) and then fed to the NI PXIe-5622. This is used as an IF digitizer, a 16-bit analog-to-digital converter, as shown in Fig. 8.

2) IF and Baseband Signal Processing: After the RF signal acquisition process, we have two digitized IF signals at the output of the respective NI PXIe-5622 IF digitizer modules. Both received digitized IF signals are input to the MATLAB script, which runs inside the LabVIEW MathScript RT module. As we use the complex baseband signals at each level of classification, the complex baseband signals are obtained by another down-conversion and filtering of the IF signals. The IF frequency is determined by coarse and fine carrier frequency estimations [4]. Finally, the MC algorithm is performed to classify all seven modulation formats, as shown in Fig. 5. For the implementation and measurement for SISO, SIMO, and MISO systems, we follow the same procedure and use the number of transmit and receive antennas accordingly. For the SISO system, the algorithm implemented in [2] requires the IF signal to classify some of the modulation formats, where the sampling rate has to be eight times the IF carrier frequency, which has been eliminated in this proposed work, as only the baseband signal is required to classify the modulation formats.

V. SIMULATION AND MEASUREMENT RESULTS

Simulations and measurements were used to evaluate the performance of the proposed MC algorithm. The simulation and experiment parameters are provided in Table I. For simulations, a Rayleigh frequency-selective fading channel is considered with $L = 4$ and 8 channel taps, respectively, and the symbol rate is varied between 1 and 5 MHz. During measurement, the RF and IF carrier frequencies are set to 2.3 GHz and 5 MHz, respectively. The receiver sampling rate is 50 MHz, which results in an oversampling factor of $P = 10$

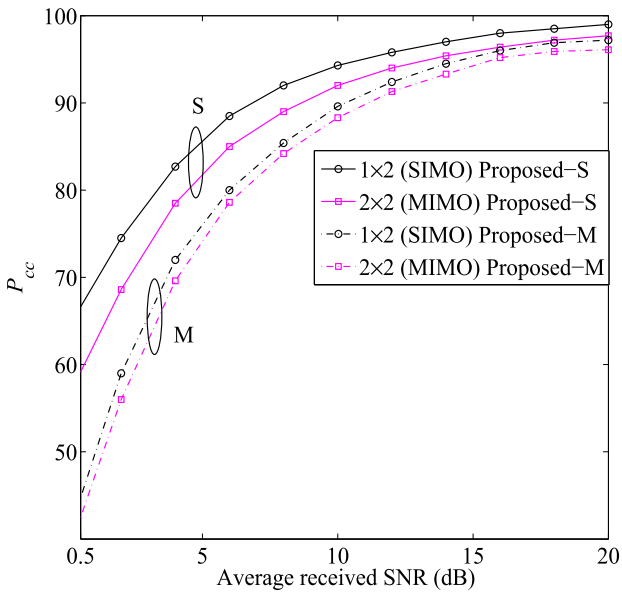

Fig. 10. Measurement (M) and simulation (S) results: P_{cc} versus SNR for (BPSK, QPSK, OQPSK, MSK, $\pi/4$-QPSK, 8-PSK, and 16-QAM) modulation formats, with different antenna configurations ($N_t = 1, 2$, $N_r = 2$).

($P = F_s/f_s = 50$ MHz/5 MHz $= 10$). We implemented the proposed algorithm for seven modulation schemes. The number of symbols for each iteration is set to 20 000, and the performance is measured from 10 000 iterations. Fig. 9 shows the LabVIEW front panel of the 2×2 MIMO transmitter setup with the transmit parameters. The constellation points are obtained for the QPSK modulation. It is observed that the constellation points are scattered around the ideal positions. This is an inevitable consequence of imperfect sampling and RRC pulse shaping filter.

Figs. 10 and 11 show the percentage of correct classification (P_{cc}) as a function of the average received signal-to-noise ratio (SNR); results are provided for the seven modulation formats and with different antenna configurations, for measurements (M) and simulations (S).

In measurements, the received SNR is calculated in two steps: first, we set the system noise floor power (decibel) at the receiver by keeping the transmitter idle. Next, we tune the power level at the transmitter as shown in Fig. 9 and calculate the signal power (decibel) at the receiver. Now, we have the received SNR in decibel (signal power—system noise floor power). In simulations, the received SNR is calculated from the received signal.

It has been observed that the simulated P_{cc} has slightly better performance as compared to the measurement. For example, at 20-dB SNR for the SIMO system, classification accuracy through simulation and measurement is 99% and 97.3%, respectively. The error percentage in simulation and measurement is 1% and 2.7%, respectively. This increases at low SNRs. The performance deviation is due to the RF mismatch that results in additional frequency offset in the IF estimation during the measurement process [4]. Moreover, another RF impairment in the NI VSG and VSA is the I/Q imbalance, such as gain imbalance, dc offset, and quadrature skew [39], which also affects the MC performance

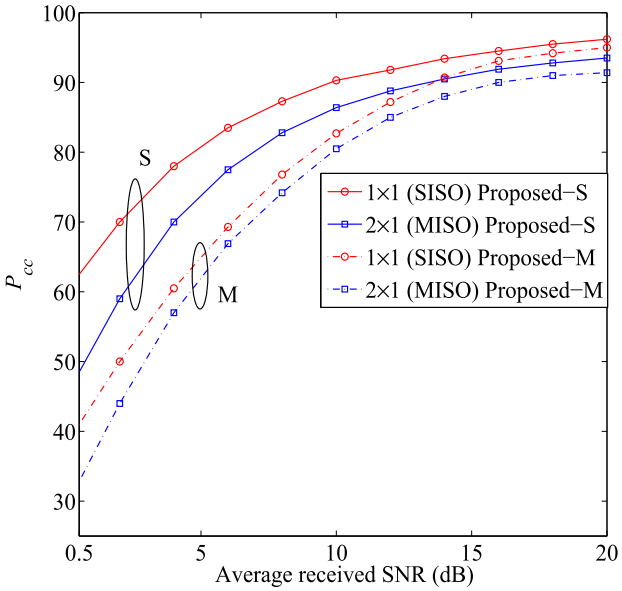

Fig. 11. Measurement (M) and simulation (S) results: P_{cc} versus SNR for (BPSK, QPSK, OQPSK, MSK, $\pi/4$-QPSK, 8-PSK, and 16-QAM) modulation formats, with different antenna configurations ($N_t = 1, 2$, $N_r = 1$).

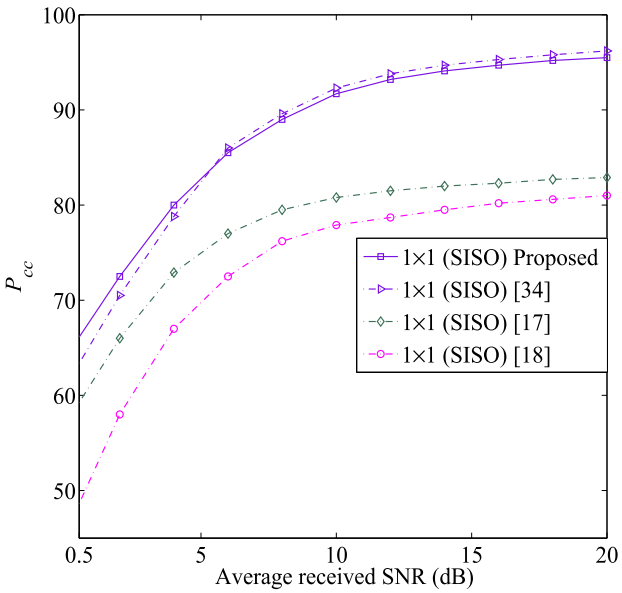

Fig. 12. Simulation results: P_{cc} versus SNR for (BPSK, QPSK, 8-PSK, and 16-QAM) for SISO systems.

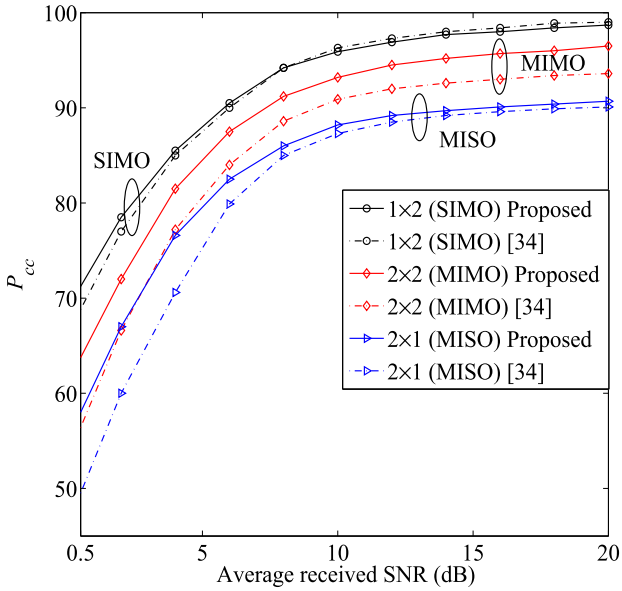

Fig. 13. Simulation results: P_{cc} versus SNR for (BPSK, QPSK, 8-PSK, and 16-QAM) for MIMO, SIMO, and MISO systems.

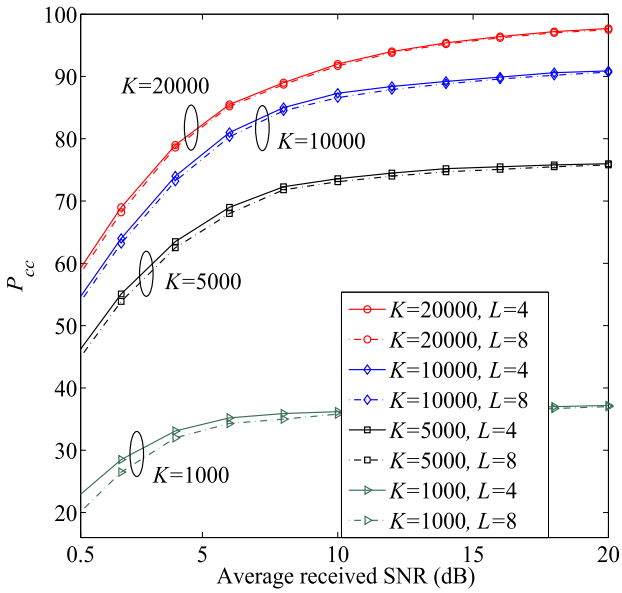

Fig. 14. Simulation results: effect of K and L on P_{cc} for 2×2 MIMO for the classification of the seven modulation formats.

in the measurement environment. In addition, by comparing results in Figs. 10 and 11, it is noted that improved results are attained for $N_r = 2$ when compared with $N_r = 1$, as expected.

Figs. 12 and 13 show the simulation result comparison of the proposed classifier with existing works. It is observed that the proposed algorithm outperforms the algorithms in [17] and [18] for the SISO system. It is also noticed that the proposed algorithm and the method in [34] have a similar performance for SISO, SIMO, and MISO. However, the method in [34] can be applied only to the classification of BPSK, QPSK, 8-PSK, and 16-QAM modulations, whereas the proposed algorithm is applicable to a larger pool of modulation formats and also works for the MIMO systems with better classification performance.

Fig. 14 shows P_{cc} as a function of SNR, for different values of K and L. A strong enhancement in the classification performance is achieved as K increases. For better classification performance, the observation length K needed for higher order statistic estimation is greater than the one required for the lower order statistics. It is also observed that the performance is independent of L. This reflects the advantage of the proposed algorithm, i.e., it does not require knowledge of CSI. From the above studies, a good performance is achieved for $K = 20\,000$ and $P = 10$. Thus, $NT_s = 4$ ms observation interval is required. It was also observed that the proposed

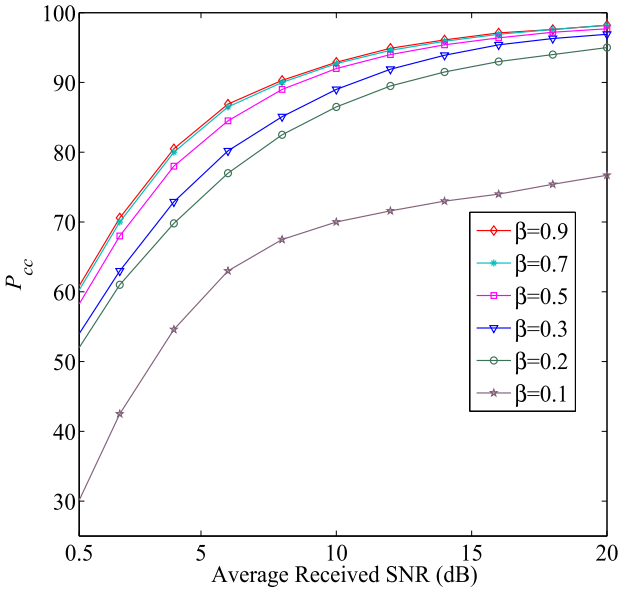

Fig. 15. Simulation results: effect of the rolloff factor (β) on P_{cc} for 2×2 MIMO for the classification of the seven modulation formats.

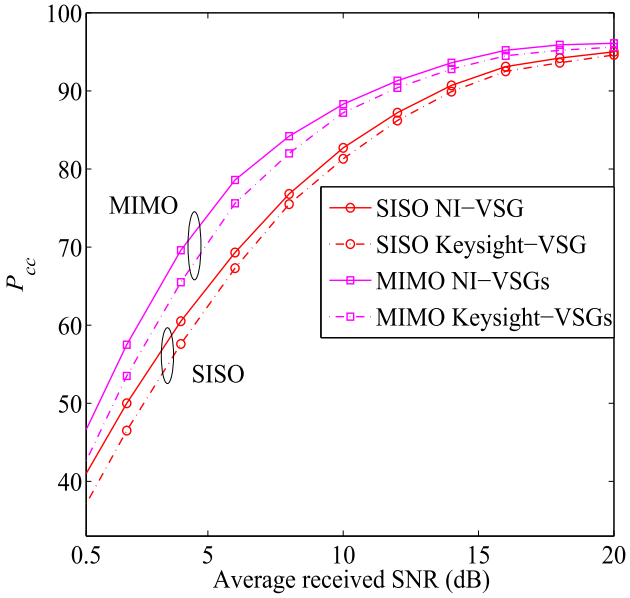

Fig. 16. Measurement results: P_{cc} versus SNR for signal generated from the NI and Keysight VSGs for SISO and MIMO systems.

algorithm works in the presence of phase and timing offset. Moreover, if a frequency offset error about $\pm 50 \sim \pm 1000$ Hz is present in the received baseband signals, it does not affect the classification performance.

Fig. 15 shows P_{cc} as a function of SNR, for different values of β. It is observed that the optimum value of the rolloff factor is between 0.3 and 0.7. The proposed algorithm uses the symbol-rate peaks to classify some of the modulation schemes, and hence, the pulse shaping is required for finding the symbol-rate feature.

Fig. 16 shows P_{cc} as a function of SNR, for the NI and Keysight VSGs. It is observed that there is a slight performance deviation, which is due to the difference in the hardware

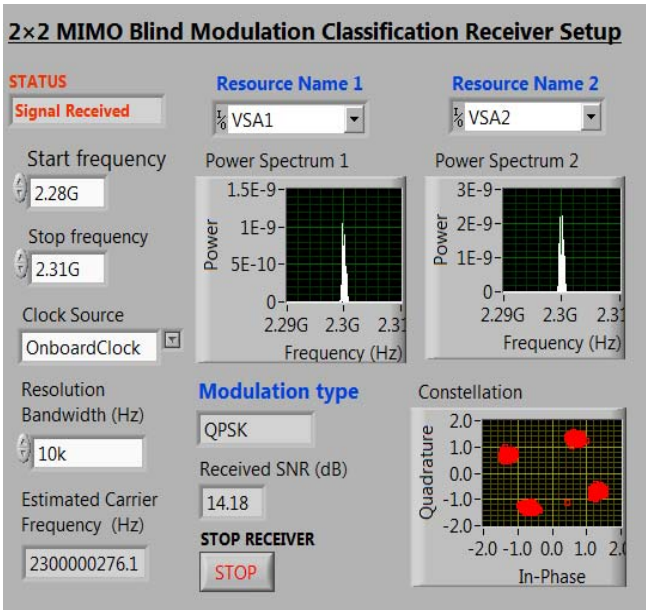

Fig. 17. LabVIEW front panel of the receiver setup using PXIe-5663 for the 2×2 MIMO system.

TABLE II
COMPLEXITY ANALYSIS

Methods	Order of Complexity
Maximum Likelihood (ML)	$\mathcal{O}(N \times M_a \times I)$
Proposed algorithm	$\mathcal{O}(N log_2 N)$
Cumulant and Correlation function	$\mathcal{O}(N)$

configuration and impairments in the NI and Keysight signal generators [39], [41].

Fig. 17 presents an instantaneous measurement performance of the proposed MC algorithm. It shows the LabVIEW front panel of the receiver using PXIe-5663 for the 2×2 MIMO system, where the modulation type, RF carrier frequency, received SNR, and constellation points are estimated. Table II compares the computational complexity of the proposed and existing algorithms.

Here, N is the received signal length, M_a is the constellation size of the ath modulation scheme, and I is the total number of modulation schemes considered for classification. The complexity of the proposed algorithm is less than of the ML algorithm but greater than that of the algorithms based on the cumulant and correlation function. Moreover, the algorithms based on the ML, cumulant, and correlation function cannot classify 8-PSK and different variants of the QPSK modulation formats, i.e., OQPSK, $\pi/4$-QPSK, and MSK.

VI. CONCLUSION

An MC algorithm has been proposed and implemented for single and multiple antenna systems and seven modulation formats, transmitted over frequency-selective fading channels. This also works in the presence of timing, phase, and frequency offsets, without having prior knowledge of the CSI.

The proposed algorithm is based on the properties of second-order correlation function, second-order CC, fourth-order correlation, and fourth-order cumulant. The measurement and simulation results show that the proposed MC algorithm can achieve adequate classification performance for SISO, SIMO, MISO, and MIMO systems in realistic scenarios and are also able to classify different variants of QPSK modulation formats, i.e., OQPSK, $\pi/4$-QPSK, and MSK.

REFERENCES

[1] O. A. Dobre, A. Abdi, Y. Bar-Ness, and W. Su, "Survey of automatic modulation classification techniques: Classical approaches and new trends," *IET Commun.*, vol. 1, no. 2, pp. 137–156, Apr. 2007.

[2] S. Majhi, R. Gupta, W. Xiang, and S. Glisic, "Hierarchical hypothesis and feature-based blind modulation classification for linearly modulated signals," *IEEE Trans. Veh. Technol.*, vol. 66, no. 12, pp. 11057–11069, Dec. 2017.

[3] Y. A. Eldemerdash, O. A. Dobre, O. Üreten, and T. Yensen, "Identification of cellular networks for intelligent radio measurements," *IEEE Trans. Instrum. Meas.*, vol. 66, no. 8, pp. 2204–2211, Aug. 2017.

[4] S. Majhi, M. Kumar, and W. Xiang, "Implementation and measurement of blind wireless receiver for single carrier systems," *IEEE Trans. Instrum. Meas.*, vol. 66, no. 8, pp. 1965–1975, Aug. 2017.

[5] O. A. Dobre, "Signal identification for emerging intelligent radios: Classical problems and new challenges," *IEEE Instrum. Meas. Mag.*, vol. 18, no. 2, pp. 11–18, Apr. 2015.

[6] S. Majhi and T. S. Ho, "Blind symbol-rate estimation and test bed implementation of linearly modulated signals," *IEEE Trans. Veh. Technol.*, vol. 64, no. 3, pp. 954–963, Mar. 2015.

[7] J. L. Xu, W. Su, and M. Zhou, "Software-defined radio equipped with rapid modulation recognition," *IEEE Trans. Veh. Technol.*, vol. 59, no. 4, pp. 1659–1667, May 2010.

[8] W. Wei and J. M. Mendel, "Maximum-likelihood classification for digital amplitude-phase modulations," *IEEE Trans. Commun.*, vol. 48, no. 2, pp. 189–193, Feb. 2000.

[9] M. E. Magana and A. Kandukuri, "Non-data-aided parametric- and nonparametric-based carrier frequency estimators for burst GMSK communication systems," *IEEE Trans. Instrum. Meas.*, vol. 59, no. 7, pp. 1783–1792, Jul. 2010.

[10] A. Aiello and D. Grimaldi, "Frequency error measurement in GMSK signals in a multipath propagation environment," *IEEE Trans. Instrum. Meas.*, vol. 52, no. 3, pp. 938–945, Jun. 2003.

[11] S. Kumar, S. Majhi, and C. Yuen, "Multi-user CFOs estimation for SC-FDMA system over frequency selective fading channels," *IEEE Access*, vol. 6, pp. 43146–43156, 2018.

[12] Q. Honglei, Q. Changquan, C. Li, and C. Yang, "Wireless LXI bus clock synchronization and triggering design," *IEEE Trans. Instrum. Meas.*, vol. 59, no. 9, pp. 2420–2430, Sep. 2010.

[13] Y. Wu, X. Zhu, Y. Huang, G. Sun, and G. Ou, "Uncertainty derivation and performance analyses of clock prediction based on mathematical model method," *IEEE Trans. Instrum. Meas.*, vol. 64, no. 10, pp. 2792–2801, Oct. 2015.

[14] P. Ferrari *et al.*, "Timestamping and ranging performance for IEEE 802.15.4 CSS systems," *IEEE Trans. Instrum. Meas.*, vol. 63, no. 5, pp. 1244–1252, May 2014.

[15] Q. Wang, Y. Tang, and M. Soma, "Method to measure RF transceiver bandwidth in the time domain," *IEEE Trans. Instrum. Meas.*, vol. 55, no. 3, pp. 982–988, Jun. 2006.

[16] A. Abdi, O. A. Dobre, R. Choudhry, Y. Bar-Ness, and W. Su, "Modulation classification in fading channels using antenna arrays," in *Proc. IEEE Mil. Commun. Conf.*, Oct./Nov. 2014, pp. 211–217.

[17] H. C. Wu, M. Saquib, and Z. Yun, "Novel automatic modulation classification using cumulant features for communications via multipath channels," *IEEE Trans. Wireless Commun.*, vol. 7, no. 8, pp. 3098–3105, Aug. 2008.

[18] V. D. Orlic and M. L. Dukic, "Automatic modulation classification algorithm using higher-order cumulants under real-world channel conditions," *IEEE Commun. Lett.*, vol. 13, no. 12, pp. 917–919, Dec. 2009.

[19] A. Swami and B. M. Sadler, "Hierarchical digital modulation classification using cumulants," *IEEE Trans. Commun.*, vol. 48, no. 3, pp. 416–429, Mar. 2000.

[20] O. A. Dobre, M. Oner, S. Rajan, and R. Inkol, "Cyclostationarity-based robust algorithms for QAM signal identification," *IEEE Commun. Lett.*, vol. 16, no. 1, pp. 12–15, Jan. 2012.

[21] P. Daponte, G. Mercurio, and S. Rapuano, "A wavelet networks-based method for the digital telecommunication system monitoring," *IEEE Trans. Instrum. Meas.*, vol. 50, no. 6, pp. 1773–1780, Dec. 2001.

[22] M. Oner and O. A. Dobre, "On the second-order cyclic statistics of signals in the presence of receiver impairments," *IEEE Trans. Commun.*, vol. 59, no. 12, pp. 3278–3284, Dec. 2011.

[23] G. B. Giannakis and G. Zhou, "Harmonics in multiplicative and additive noise: Parameter estimation using cyclic statistics," *IEEE Trans. Signal Process.*, vol. 43, no. 9, pp. 2217–2221, Sep. 1995.

[24] W. A. Jerjawi, Y. A. Eldemerdash, and O. A. Dobre, "Second-order cyclostationarity-based detection of LTE SC-FDMA signals for cognitive radio systems," *IEEE Trans. Instrum. Meas.*, vol. 64, no. 3, pp. 823–833, Mar. 2015.

[25] O. A. Dobre, Y. Bar-Ness, and W. Su, "Higher-order cyclic cumulants for high order modulation classification," in *Proc. IEEE Mil. Commun. Conf.*, Oct. 2003, pp. 112–117.

[26] M. Kim, J. I. Takada, and Y. Konishi, "Novel scalable MIMO channel sounding technique and measurement accuracy evaluation with transceiver impairments," *IEEE Trans. Instrum. Meas.*, vol. 61, no. 12, pp. 3185–3197, Dec. 2012.

[27] A. Taparugssanagorn and J. Ylitalo, "Characteristics of short-term phase noise of MIMO channel sounding and its effect on capacity estimation," *IEEE Trans. Instrum. Meas.*, vol. 58, no. 1, pp. 196–201, Jan. 2009.

[28] Y. A. Eldemerdash, O. A. Dobre, and M. Öner, "Signal identification for multiple-antenna wireless systems: Achievements and challenges," *IEEE Commun. Surveys Tuts.*, vol. 18, no. 3, pp. 1524–1551, 3rd Quart., 2016.

[29] X. Liu, C. Zhao, P. Wang, Y. Zhang, and T. Yang, "Blind modulation classification algorithm based on machine learning for spatially correlated MIMO system," *IET Commun.*, vol. 11, no. 7, pp. 1000–1007, May 2017.

[30] Z. Zhu and A. K. Nandi, "Blind modulation classification for MIMO systems using expectation maximizatio," in *Proc. IEEE Mil. Commun. Conf.*, Oct. 2014, pp. 754–759.

[31] K. Hassan, I. Dayoub, W. Hamouda, C. N. Nzeza, and M. Berbineau, "Blind digital modulation identification for spatially-correlated MIMO systems," *IEEE Trans. Wireless Commun.*, vol. 11, no. 2, pp. 683–693, Feb. 2012.

[32] M. S. Muhlhaus, M. Oner, O. A. Dobre, and F. K. Jondral, "A low complexity modulation classification algorithm for MIMO systems," *IEEE Commun. Lett.*, vol. 17, no. 10, pp. 1881–1884, Oct. 2013.

[33] M. S. Mühlhaus, M. Öner, O. A. Dobre, H. U. Ükel, and F. K. Jondral, "Automatic modulation classification for MIMO systems using fourth-order cumulants," in *Proc. IEEE Veh. Technol. Conf. (VTC Fall)*, Sep. 2012, pp. 1–5.

[34] M. Marey and O. A. Dobre, "Blind modulation classification algorithm for single and multiple-antenna systems over frequency-selective channels," *IEEE Signal Process. Lett.*, vol. 21, no. 9, pp. 1098–1102, Sep. 2014.

[35] M. Marey and O. A. Dobre, "Blind modulation classification for alamouti STBC system with transmission impairments," *IEEE Wireless Commun. Lett.*, vol. 4, no. 5, pp. 521–524, Oct. 2015.

[36] Y. Yao and G. B. Giannakis, "Blind carrier frequency offset estimation in SISO, MIMO, and multiuser OFDM systems," *IEEE Trans. Commun.*, vol. 53, no. 1, pp. 173–183, Jan. 2005.

[37] S. Majhi, R. Gupta, and W. Xiang, "Novel blind modulation classification of circular and linearly modulated signals using cyclic cumulants," in *Proc. IEEE Int. Symp. Pers., Indoor, Mobile Radio Commun.*, Oct. 2017, pp. 1–5.

[38] R. Gupta, S. Majhi, and O. A. Dobre, "Blind modulation classification of different variants of QPSK and 8-PSK for multiple-antenna systems with transmission impairments," in *Proc. IEEE Veh. Technol. Conf. (VTC Fall)*, Aug. 2018.

[39] National Instruments, Bengaluru, India. (2018). *National Instruments PXI platform*. [Online]. Available: http://www.ni.com

[40] T. S. Rappaport, *Wireless Communications: Principles and Practice* (Prentice Hall Communications Engineering and Emerging Technologies Series), 2nd ed. New York, NY, USA: Pearson, 2002.

[41] Keysight Technologies, Bengaluru, India. (2018). *Keysight PXI Platform*. [Online]. Available: http://www.keysight.com

Rahul Gupta received the B.Tech. degree in electronics and communication from the Oriental Institute of Science and Technology, Bhopal, India, in 2012, and the M.Tech. degree in communication system engineering from IIT Patna, Patna, India, in 2015, where he is currently pursuing the Ph.D. degree in electrical engineering.

His current research interests include signal processing, wireless communication, estimation and detection theory, higher order statistics, orthogonal frequency-division multiplexing (OFDM), multiple-input multiple-output (MIMO), and MIMO-OFDM and their applications in blind modulation classification and parameters estimation.

Sudhan Majhi (SM'16) received the M.Tech. degree in computer science and data processing from IIT Kharagpur, Kharagpur, India, in 2004, and the Ph.D. degree from Nanyang Technological University, Singapore, in 2008.

He is currently an Associate Professor with the Department of Electrical Engineering, IIT Patna, Patna, India, where he is a Fellow of Sir Visvesvaraya Young Faculty Research. He has a postdoctoral experience with the University of Michigan, Dearborn, MI, USA; Institute of Electronics and Telecommunications, Rennes, France; and Nanyang Technological University, Singapore. His current research interests include signal processing for wireless communication which includes blind synchronization and parameter estimation, cooperative communications, physical layer security for cognitive radio, sequence design, orthogonal frequency-division multiplexing (OFDM), multiple-input multiple-output (MIMO), single carrier-frequency division multiple access, and MIMO-OFDM.

Octavia A. Dobre (M'05–SM'07) received the Dipl. Ing. and Ph.D. degrees from the Politehnica University of Bucharest, Bucharest, Romania, in 1991 and 2000, respectively.

From 2002 to 2005, she was with the Politehnica University of Bucharest and New Jersey Institute of Technology, Newark, NJ, USA. In 2005, she joined Memorial University, St. John's, NL, Canada, where she is currently a Professor and the Research Chair. In 2013, she was a Visiting Professor with the Université de Bretagne Occidentale, Brest, France, and Massachusetts Institute of Technology, Cambridge, MA, USA. Her current research interests include 5G enabling technologies, blind signal identification, and parameter estimation techniques, as well as optical and underwater communications among others.

Dr. Dobre is a Fellow of the Engineering Institute of Canada. She serves as the Editor-in-Chief of IEEE COMMUNICATIONS LETTERS, as well as an Editor of the IEEE SYSTEMS and IEEE COMMUNICATIONS SURVEYS AND TUTORIALS. She was an Editor, a Senior Editor, and a Guest Editor for other prestigious journals. She served as the General Chair, the Tutorial Co-Chair, and the Technical Co-Chair at numerous conferences. She was a Royal Society Scholar in 2000 and a Fulbright Scholar in 2001.